Mass-specific scattering cross sections of suspended sediments and aggregates: theoretical limits and applications

Robert H. Stavn*

Department of Biology, P.O. Box 26174, University of North Carolina, Greensboro, NC 27402, USA
*stavnr@uncg.edu

Abstract: The spectral mass-specific scattering cross section $\sigma_{[PIM]}(\lambda)$ is most important for the remote sensing inversion of the concentration of suspended mineral matter in the coastal ocean. This optical parameter is also important in optical theory and therefore the theoretical limits of this parameter are important. There are differing reports in the literature on the magnitude of $\sigma_{[PIM]}(\lambda)$ and its spectral slope in different coastal ocean systems. To account for and predict these differences, I have applied a model of the size distribution of primary suspended mineral particles and aggregates of these particles to theoretical calculations of $\sigma_{[PIM]}(\lambda)$. I utilized a model of mineral particle aggregates by Khelifa and Hill [Khelifa, A. and P.S. Hill, J. Hydraul. Res. 44, 390 (2006)] and Latimer's optical model of aggregates [Latimer, P., Appl. Opt. 24, 3231, (1985)]. I have been able to account for the variations in magnitude and spectral slope of $\sigma_{[PIM]}(\lambda)$. This analysis will apply to not only inverting the concentration of suspended mineral matter but also provides the basis for inverting the processes of coagulation and aggregation of primary mineral particles in determining sedimentation rates, budgets, etc.

OCIS Codes: (010.4450) Oceanic optics; (010.4458) Oceanic scattering; (290.5850) Scattering, particles; (290.4020) Mie theory; (000.4430) Numerical approximation and analysis.

References and Links

1. R. W. Gould, Jr. and R. A. Arnone, "Three-dimensional modelling of inherent optical properties in a coastal environment: coupling ocean colour imagery and *in situ* measurements," Int. J. Remote Sens. **19**(11), 2141–2159 (1998).
2. R. W. Gould, Jr., R. A. Arnone, and M. Sydor, "Absorption, scattering, and remote-sensing reflectance relationships in coastal waters: testing a new inversion algorithm," J. Coast. Res. **17**(2), 328–341 (2001).
3. R. W. Gould, Jr., R.H, Stavn, M. S. Twardowski, and G.M. Lamela. "Partitioning optical properties into organic and inorganic components from ocean color imagery," in *Ocean Optics XVI, Santa Fe, New Mexico, USA*, S. Ackleson and C. Trees, eds. (Office of Naval Research, 2002) CDROM.
4. M. Sydor, R. W. Gould, R. A. Arnone, V. I. Haltrin, and W. Goode, "Uniqueness in remote sensing of the inherent optical properties of ocean water," Appl. Opt. **43**(10), 2156–2162 (2004).
5. J. S. Cleveland, "Regional models for phytoplankton absorption as a function of chlorophyll *a* concentration," J. Geophys. Res. **100**(C7), 13,333–13,344 (1995).
6. R. H. Stavn and S. J. Richter, "Biogeo-optics: particle optical properties and the partitioning of the spectral scattering coefficient of ocean waters," Appl. Opt. **47**(14), 2660–2679 (2008).
7. R. H. Stavn and T. R. Keen, "Suspended minerogenic particle distributions in high-energy coastal environments: Optical implications," J. Geophys. Res. **109**(C5), C05005 (2004), doi:10.1029/2003JC002098 (Oceans).
8. R. P. Bukata, J. H. Jerome, K. Ya. Kondratyev, and D. V. Pozdnayakov, *Optical Properties and Remote Sensing of Inland and Coastal Waters* (CRC Press 1995).
9. E. A. Laws and J. W. Archie, "Appropriate use of regression analysis in marine biology," Mar. Biol. **65**(1), 13–16 (1981).
10. R. A. Green, H. M. Sosik, and R. J. Olson, "Contributions of phytoplankton and other particles to inherent optical properties in New England continental shelf waters," Limnol. Oceanogr. **48**(6), 2377–2391 (2003).
11. I. N. Sokolik and O. B. Toon, "Incorporation of mineralogical composition into models of the radiative properties of mineral aerosol from UV to IR wavelengths," J. Geophys. Res. **104**(D8), 9423–9444 (1999).

#155094 - $15.00 USD Received 20 Sep 2011; revised 18 Nov 2011; accepted 1 Dec 2011; published 20 Dec 2011

12. E. Boss, W. Slade, and P. Hill, "Effect of particulate aggregation in aquatic environments on the beam attenuation and its utility as a proxy for particulate mass," Opt. Express **17**(11), 9408–9420 (2009).
13. R. A. Reynolds, D. Stramski, V. M. Wright, and S. B. Woźniak, "Measurements and characterization of particle size distributions in coastal waters," J. Geophys. Res. **115**(C8 C08024), C08024 (2010), doi:10.1029/2009JC005930.
14. H. Bader, "The hyperbolic distribution of particle sizes," J. Geophys. Res. **75**(15), 2822–2830 (1970).
15. M. Jonasz and G. R. Fournier, *Light Scattering by Particles in Water* (Academic/Elsevier 2007).
16. C. Lambert, C. Jehanno, N. Silverberg, J. C. Brun-Cottan, and R. Chesselet, "Log-normal distributions of suspended particles in the open ocean," J. Mar. Res. **39**, 77–98 (1981).
17. F. Peng, S. W. Effler, D. O'Donnell, M. G. Perkins, and A. Weidemann, "Role of minerogenic particles in light scattering in lakes and a river in central New York," Appl. Opt. **46**(26), 6577–6594 (2007).
18. F. Peng, S. Effler, D. O'Donnell, A. Weidemann, and M. T. Auer, "Characterization of minerogenic particles in support of modeling light scattering in Lake Superior through a two-component approach," Limnol. Oceanogr. **54**(4), 1369–1381 (2009).
19. M. Stramska, D. Stramski, M. Cichocka, A. Cieplak, and S. B. Wozniak, "Effects of atmospheric particles from Southern California on the optical properties of seawater," J. Geophys. Res. **113**(C8), C08037 (2008), doi:10.1029/2007JC004407.
20. D. Stramski, S. B. Wozniak, and P. J. Flatau, "Optical properties of Asian mineral dust suspended in seawater," Limnol. Oceanogr. **49**(3), 749–755 (2004).
21. D. Stramski, M. Babin, and S. B. Wozniak, "Variations in the optical properties of terrigenous mineral-rich particulate matter suspended in seawater," Limnol. Oceanogr. **52**(6), 2418–2433 (2007).
22. D. Risović and M. Martinis, "The role of coagulation and sedimentation mechanisms in the two-component model of sea-particle size distribution," Fizika B: J. Exp. Theoret. Phys. (Zagreb, Croatia) **2**, 103–118 (1994).
23. M. Jonasz and G. Fournier, "Approximation of the size distribution of marine particles by a sum of log-normal functions," Limnol. Oceanogr. **41**(4), 744–754 (1996).
24. D. Risović, "Two component model of sea particle size distribution," Deep Sea Res. Part I Oceanogr. Res. Pap. **40**(7), 1459–1473 (1993).
25. J. W. Campbell, "The lognormal distribution as a model for bio-optical variability in the sea," J. Geophys. Res. **100**(C7), 13237–13254 (1995).
26. O. Ulloa, S. Sathyendranath, T. Platt, and R. A. Quinones, "Light scattering by marine heterotrophic bacteria," J. Geophys. Res. **97**(C6), 9619–9629 (1992).
27. K. Mahmood, "Lognormal size distribution of particulate matter," J. Sediment. Petrol. **43**(4), 1161–1166 (1973).
28. D. Deirmendjian, "Scattering and polarizaton properites of water clouds and hazes in the visible and infrared," Appl. Opt. **3**(2), 187–196 (1964).
29. D. Deirmendjian, *Electromagnetic Scattering on Spherical Polydispersions* (Elesevier 1969).
30. W. Zdunkowski, T. Trautman, and A. Bott, *Radiation in the Atmosphere: A Course in Theoretical Meterology*. (Cambridge 2007).
31. P. Latimer, "Experimental tests of a theoretical method for predicting light scattering by aggregates," Appl. Opt. **24**(19), 3231–3239 (1985).
32. A. Khelifa and P. S. Hill, "Models for effective density and settling velocity of flocs," J. Hydraul. Res. **44**(3), 390–401 (2006).
33. D. Risović and M. Martinis, "Fractal dimensions of suspended particles in seawater," J. Colloid Interface Sci. **182**(1), 199–203 (1996).
34. A. Morel, "Optics of marine particles and marine optics," in *Particle Size Analysis*, S. Demers, ed. (Springer Verlag, 1991), pp. 141–188.
35. I. N. McCave, "Local and global aspects of the bottom nepheloid layers in the world ocean," Neth. J. Sea Res. **20**(2-3), 167–181 (1986).
36. P. S. Hill, G. Voulgaris, and J. H. Trowbridge, "Controls on floc size in a continental shelf bottom boundary layer," J. Geophys. Res. **106**(C5), 9543–9549 (2001).
37. D. G. Bowers and C. E. Binding, "The optical properties of mineral suspended particles: A review and synthesis," Estuar. Coast. Shelf Sci. **67**(1-2), 219–230 (2006).
38. D. M. McKee and A. Cunningham, "Identification and characterization of two optical water types in the Irish Sea from in situ inherent optical properties and seawater constituents," Estuar. Coast. Shelf Sci. **68**(1-2), 305–316 (2006).
39. R. W. Gould, Jr., R. A. Arnone, and P. M. Martinolich, "Spectral dependence of the scattering coefficient in case 1 and case 2 waters," Appl. Opt. **38**(12), 2377–2383 (1999).
40. M. Sydor and R. A. Arnone, "Effect of suspended particulate and dissolved organic matter on remote sensing of coastal and riverine waters," Appl. Opt. **36**(27), 6905–6912 (1997).
41. D. M. Etter, *Fortran 77: with Numerical Methods for Engineers and Scientists* (Benjamin/Cummings 1992).
42. O. Atteia, D. Perret, T. Adatte, R. Kozel, and P. Rossi, "Characterization of natural colloids from a river and spring in a karstic basin," Enviorn. Geol. **34**(4), 257–269 (1998).
43. J. Buffle and G. G. Leppard, "Characterization of aquatic colloids and macromolecules. 1. structure and behavior of colloidal material," Environ. Sci. Technol. **29**(9), 2169–2175 (1995).
44. C. L. Gallegos and R. G. Menzel, "Submicron size distribution of inorganic suspended solids in turbid waters by photon correlation spectroscopy," Water Resour. Res. **23**(4), 596–602 (1987).

#155094 - $15.00 USD Received 20 Sep 2011; revised 18 Nov 2011; accepted 1 Dec 2011; published 20 Dec 2011

45. Q. Jiang and B. E. Logan, "Fractal dimensions of aggregates determined from steady-state size distributions," Environ. Sci. Technol. **25**(12), 2031–2038 (1991).
46. T. A. Witten and M. E. Cates, "Tenuous structures from disorderly growth processes," Science **232**(4758), 1607–1612 (1986).
47. L. J. Doyle and T. N. Sparks, "Sediments of the Mississippi, Alabama, and Florida (MAFLA) continental shelf," J. Sediment. Petrol. **50**, 905–916 (1980).
48. W.G. Egan and T.W. Hilgeman, *Optical Properties of Inhomogeneous Materials* (Academic 1979).
49. P. Fleischer, "Mineralogy and sedimentation history, Santa Barbara basin, California," J. Sediment. Petrol. **42**(1), 49–58 (1972).
50. A. G. Johnson and J. T. Kelley, "Temporal, spatial, and textural variation in the mineralogy of Mississippi river suspended sediment," J. Sediment. Petrol. **54**, 67–72 (1984).
51. C.F. Bohren and D.R. Huffman, *Absorption and Scattering of Light by Small Particles* (Wiley 1983).
52. J. B. Austin, "Methods of representing distribution of particle size," Ind. Eng. Chem. Anal. Ed. **11**(6), 334–339 (1939).
53. E. Aas, "Refractive index of phytoplankton derived from its metabolite composition," J. Plankton Res. **18**(12), 2223–2249 (1996).
54. C. E. Binding, D. G. Bowers, and E. G. Mitchelson-Jacob, "An algorithm for the retrieval of suspended sediment concentrations in the Irish Sea from SeaWiFS ocean colour satellite imagery," Int. J. Remote Sens. **24**(19), 3791–3806 (2003).
55. A. H. Barnard, W. S. Pegau, and J. R. V. Zaneveld, "Global relationships of the inherent optical properties of the oceans," J. Geophys. Res. **103**(C11), 24955–24968 (1998).
56. H. R. Gordon and T. Du, "Light scattering by nonspherical particles: application to coccoliths detached from *Emiliania huxleyi*," Limnol. Oceanogr. **46**(6), 1438–1454 (2001).

1. Introduction

The scattering coefficient of the marine hydrosol is the source of remote sensing information about the suspended components in the ocean and the basis for mechanistic algorithms to invert the remote sensing reflectance and retrieve concentrations of materials of interest: suspended sediments, organic particulate matter, dissolved organic matter, chlorophyll concentration, etc [1–3]. The absorption coefficient of the marine hydrosol is routinely coupled with the scattering coefficient to generate remote sensing algorithms [4]. Furthermore the absorption coefficient is routinely partitioned by various methods into absorption due to phytoplankton, yellow substance, organic detritus, etc. to give more information about the materials suspended in the marine hydrosol [1,5]). However, the scattering coefficient is not routinely partitioned except to attribute scattering to molecular water and "particles." Suspended particulate matter can be broadly classified into inorganic, often terrigenous, matter and organic matter, some terrigenous but usually autochthonous. The two broad categories of suspended particulates have different indices of refraction and therefore rather different scattering coefficients. These differing scattering coefficients generate different effects on the remote sensing reflectance. This factor is most pronounced in coastal ocean waters and our program in biogeo-optics is now making contributions to coastal ocean remote sensing algorithms by the accurate partitioning of the particulate scattering coefficient [6].

The method of Stavn and Richter [6] is a direct mechanism for partitioning the particulate scattering coefficient from the determination of the concentrations of suspended mineral and organic matter in the marine hydrosol. Various attempts to partition the particulate scattering coefficient utilized more indirect information to accomplish this. Stavn and Keen [7] did this on the basis of the biogeo-optical model in which the majority of hydrosol absorption was ascribed to chlorophyll and/or CDOM while total scattering was ascribed primarily to mineral matter. Complex nonlinear optimizations have been performed utilizing information on the remote sensing reflectance and concentrations of various modes of suspended matter [8]. Stavn and Richter [6] perform linear multiple regression of the particulate scattering coefficient against the concentrations of particulate inorganic matter (PIM) and particulate organic matter (POM), determined by loss-on-ignition analysis. The linear multiple regression applied is a new Model II type multiple regression that is valid where all the variables contain error and the independent variables are not controlled [6,9]. This new multiple regression yields partial regression coefficients of PIM and POM against the particulate scattering

#155094 - $15.00 USD Received 20 Sep 2011; revised 18 Nov 2011; accepted 1 Dec 2011; published 20 Dec 2011

coefficient which can be interpreted as mass-specific optical scattering cross sections [6]. These optical scattering cross sections plus the mass concentrations of mineral and organic matter can then be used to partition the particulate scattering coefficient into its major components, i.e. the scattering coefficient of suspended mineral matter and the scattering coefficient of suspended organic matter. PIM and POM can in principle be further partitioned to allow any number of functional relations between known inorganic and organic constituents and the particulate scattering coefficient.

The spectral mass-specific scattering cross section [6] for suspended mineral matter $\sigma_{[PIM]}(\lambda)$ has many uses. Much of the utility comes from the fact that the spectral mass-specific scattering cross section can be analyzed with the full power of optical theory. In addition, suspended mineral matter can be considered a semi-conservative oceanographic property, as is done with yellow substance (CDOM). Once suspended mineral matter has been added to the hydrosol by erosion, resuspension, etc. it acts as a conservative property. Suspended organic matter, however, is notoriously non-conservative (because of phytoplankton growth and blooms) and thus much more difficult to analyze. Furthermore, suspended mineral matter is the dominant optical component of much of the coastal ocean [6,10], the forcing function controlling a significant proportion of the optical environment, both for the emerging in-water signal in the visible region and the emerging "bright pixel" signal from the red/far-red region of the spectrum [11] that invalidates the "dark pixel" assumption of most remote sensing atmospheric correction algorithms. The mineral mass-specific scattering cross section can be used in remote sensing inversions to retrieve the mass concentration of suspended mineral matter. I will show that the spectral slope of this optical parameter appears to be useful for retrieving the state of aggregation of suspended minerals and the probable modal size of suspended mineral matter.

Suspended fine-grained mineral matter is important in transporting adsorbed organic matter, chemical nutrients, and chemical contaminants. Particle size distribution (PSD) and composition determine time of suspension and transport of materials in estuarine and coastal systems. State of aggregation affects the settling velocity of mineral particulates through changes in relative porosity and thereby density. All of this affects the contribution of suspended mineral matter to biogeochemical cycles. Thus, it is important to be able to determine in field surveys the probable median or modal size of suspended matter and its state of aggregation. The state of aggregation is important because the porosity of the aggregate changes the density of the aggregate, its refractive index, and therefore its optical properties [12].

Theoretical optical relations of suspended matter proposed by Stavn and Richter [6] illustrate the interrelations of a particle's size, density, refractive index, and scattering cross section that generate $\sigma_{[PIM]}(\lambda)$. They propose that $\sigma_{[PIM]}(\lambda)$, determined from field measurements of the particle scattering coefficient and mass concentration of mineral matter, is an optical property of a "mean mineral particle," averaged over all mineral species in suspension. This mean mineral particle can then be characterized by the known optical properties of minerals, density and refractive index, to yield a true optical scattering cross section of the mean particle. An advantage of analysis of suspended minerals is their optical properties (density and refractive index) tend to be similar and thus easy to characterize (Table 2). An analysis of mineral optical cross sections was also applied by Green et al. [10] for characterizing mineral particulates determined from flow cytometry counts of total suspended particulates in the New England continental shelf waters. Our theoretical determinations for $\sigma_{[PIM]}(\lambda)$ can be checked by quantitatively analyzing the mineral species in suspension through such techniques as X-ray diffraction and Energy Dispersive Spectra from the samples filtered from the coastal marine hydrosol. These data allow the analysis of the changes in $\sigma_{[PIM]}(\lambda)$ attributable to changes in the mineral component. Additionally, field determinations of particle size spectra will allow further analysis of the mass-specific scattering cross section against predictions made from standard particle size distribution

#155094 - $15.00 USD Received 20 Sep 2011; revised 18 Nov 2011; accepted 1 Dec 2011; published 20 Dec 2011

(PSD) models. The information we have at present indicates that laser-based particle sizing appears to have the best chance of not disturbing delicate structures of aggregates [12,13].

A primary requisite to calculating the theoretical limits on the mass-specific scattering cross section is the PSD. Numerous observations on PSD over several decades by many researchers have resulted in an agreed general exponential decrease or power law for particle concentrations as we go from smaller to larger particles, early enunciated well by Bader [14]. He hypothesized that the slope of the power law formulation of the log transformed PSD was constant. The latest information on PSD's in coastal waters, inland waters, some open ocean waters, and laboratory investigations [10, 13–21], especially mineral PSD's, indicates that the slope of the log transformed PSD is not constant but rather a function of the size of particle [22]

$$\mathrm{d}N(r) = Cr^{m(r)}\mathrm{d}r, \tag{1}$$

where $\mathrm{d}N(r)$ is the number concentration per cm^3 in the interval r, $r + \mathrm{d}r$, and C is a constant related to the concentration of particles. Equation (1) is a generalized formulation only. Actual realistic slopes of the PSD can be quite complex. At present, at least two general formulations have been proposed to explain the variations in the power law exponent of the empirical particle size distribution: Jonasz and Fournier [23] and Risović [24]. Jonasz and Fournier [23] propose that the power law behavior of the marine particle PSD results from a summation of individual component particles, each component following a lognormal distribution. Thus, the slope of the total summed particles is no longer constant but will change, based on the individual particle distributions at a given size interval of the PSD. Risović [24] proposed that this same behavior is the result of the summation of individual component distributions, each individual component following a gamma distribution. Both distributions, lognormal and gamma, describe entities in which the particle size distribution is skewed to larger numbers on the short side of a modal size class and lower numbers on the larger side of the modal class. The particles that are skewed to larger sizes than the modal size class are distributed over more size classes and there are fewer particles per size class. Many observations confirm this formulation of the distribution of size classes of individual particle types. Sokolik and Toon [11] have modeled radiative transfer in the atmosphere by treating the individual components of mineral dust as lognormally distributed. Campbell [25] has reported on the lognormal character of suspended phytoplankton and Ulloa et al. [26] have reported on suspended bacterial particles exhibiting a gamma distribution. Mahmood [27] reports on the lognormal distribution of mineral matter, both suspended and in sediments. Risović and Martinis [22] have shown that the gamma distribution shape parameters can be applied directly to the $m(r)$ exponent of Eq. (1). Risović and Martinis [22] have further demonstrated that the exponent $m(r)$ in Eq. (1) is the result of the type of coagulation or aggregation process of primary particles into amorphous particle aggregates.

Risović [24], in an extensive analysis of published PSD's, has proposed a model of particle size distribution in the sea made up of two components: component A (small sized) and component B (large sized), each described by 3 parameters of a generalized or extended gamma distribution. The extended gamma distribution has been well described by Deirmendjian [28,29] and Zdunkowski et al. [30]. The parameters of the two-component model published by Risović [24] describe a summation of all the gamma-distributed particle components in the ocean. They provide a useful starting point for analyzing the distribution of subsets of the total array of materials suspended in the ocean. Peng, et al. [17,18] have successfully applied extended gamma distribution parameters for the B component to the PSD of suspended minerals in freshwater lakes and rivers. An advantage of the gamma distribution is the distribution shape and location parameters associated with it that help in the description and visualization of a particle size distribution. For this study of the optical properties of

#155094 - $15.00 USD Received 20 Sep 2011; revised 18 Nov 2011; accepted 1 Dec 2011; published 20 Dec 2011

suspended minerals in the coastal ocean I have chosen the power and flexibility of Risović's approach for the PSD derived for this analysis.

When considering the effects of suspended mineral matter on the optics of coastal ocean waters, there is increasing attention being given to the coagulation of small mineral particles (approximately 1 μm diameter) into larger amorphous aggregates. Boss et al. [12] point out the significance of mineral particulate aggregations and discuss their effects on some optical properties of suspended minerals and their aggregates. The aggregation of smaller mineral particles is significant because in a mineral aggregate the optical properties can no longer be modeled with unmodified Mie scattering theory. For example, the porosity of the mineral aggregate means that optically the aggregate becomes a mixture of mineral properties and water properties. Latimer [31], however, has proposed a simple optical theory for aggregate particles that involves Mie calculations for a coated sphere, the outer layer being the sum of the mineral mass of the aggregate and inner core being water. I have been able to apply the conclusions of Latimer to determine the theoretical optical properties of the mineral aggregate and its contribution to the mineral mass-specific scattering cross section $\sigma_{[PIM]}(\lambda)$. I have chosen the model of Khelifa and Hill [32], favored by Boss et al. [12], for modeling mineral particle aggregates. The Khelifa-Hill model describes the aggregate as a fractal entity composed of smaller primary particles, such as clay particles of about 1 μm diameter or so. Risović and Martinis [33] have explored the interrelations of the fractal nature of suspended aggregates and the two-component model [24] of particle size distribution in the sea. The formation and breakup of aggregations is known to affect the particle scattering coefficient. The relative increase or decrease of total particles will correspondingly affect the magnitude of the particle scattering coefficient [12,34,35]. Furthermore, the tendency to scavenge either all particles equally or to remove some particle size classes preferentially will change the PSD. This will then affect the spectral scattering slope of the particle scattering coefficient [36]. The size range of suspended particles that will have the strongest effect on the particle scattering coefficient will be those of < 10 μm diameter [34].

The purpose of this exercise is to explore the theoretical optical properties of the mineral mass-specific scattering cross section and how they are affected by suspended mineral aggregates. This is inspired in part by the divergence of mineral mass-specific scattering cross section results reported by Stavn and Richter [6] for Mobile Bay,Alabama, USA and Southwest Pass, mouth of the Mississippi River, USA and by Bowers and Binding [37] and McKee and Cunningham [38] for the Irish Sea, UK. The results will be compared with literature values on the optical properties of air dust suspensions in seawater [19–21]. These results will also have a bearing on the issue of whether or not there is a spectral slope to the particle scattering coefficient in the ocean [39].

2. Methods

I utilized a PSD reported by Sydor and Arnone [40] from St. Louis Bay, Mississippi, USA as a "template" on which to fit the PSD model, the extended gamma distribution as exemplified by the Risović [24] two-component model which consists of

$$\begin{aligned} &\mathrm{d}N(r) = C_A F_A(r)\mathrm{d}r + C_B F_B(r)\mathrm{d}r, \\ &F_A(r) = r^{\mu_A}\exp\left(-b_A r^{\gamma_A}\right),\ F_B(r) = r^{\mu_B}\exp\left(-b_B r^{\gamma_B}\right), \end{aligned} \tag{2}$$

where $\mathrm{d}N(r)$ the number of particles per cm^3 in the interval of radius r, $r + \mathrm{d}r$ or Δr μm, C_A, C_B cm^{-3} $\mu\mathrm{m}^{-3}$ are scale parameters related to the concentration of the A component (smaller particles) and B component (larger particles), μ_A and μ_B are parameters related to the modal values of the distributions of the two particle components, b_A $\mu\mathrm{m}^{-1}$ and b_B $\mu\mathrm{m}^{-1}$ are parameters of the width the of distribution of each component, and γ_A and γ_B are the shape parameters of each particle component's distribution. The A component exhibits a "steeper" shaped size distribution than the B component which exhibits a "flatter" shaped size

#155094 - $15.00 USD Received 20 Sep 2011; revised 18 Nov 2011; accepted 1 Dec 2011; published 20 Dec 2011

distribution. The γ parameters are the most variable components of the model. They are varied to generate the different types of distributions of the A component and the B component. They help determine whether there are relatively more or less smaller particles present. Any numerical concentration of any size range of the A component is determined in the same way as in a size range of the B component. For any radius interval $r_i = r_u - r_l = \Delta r$, where r_u is the upper bound of the interval and r_l is the lower bound of the interval, the particle concentration in a particular size range of this model is evaluated as follows

$$N_{Ai} = C_A \int_{-\Delta/2}^{+\Delta r/2} F_A(r_i)\,\mathrm{d}r = C_A \int_{-\Delta/2}^{+\Delta r/2} r_i^{\mu_A} e^{-b_A r_i^{\gamma_A}}\,\mathrm{d}r,$$
$$N_A = \sum_i N_{Ai}, \tag{3}$$

$$N_{Bi} = C_B \int_{-\Delta/2}^{+\Delta r/2} F_B(r_i)\,\mathrm{d}r = C_B \int_{-\Delta/2}^{+\Delta r/2} r_i^{\mu_B} e^{-b_B r_i^{\gamma_B}}\,\mathrm{d}r,$$
$$N_B = \sum_i N_{Bi}, \tag{4}$$

$$N_T = N_A + N_B, \tag{5}$$

where N_A is the total number of A component particles, N_B is the total number of B component particles, and N_T is the total particle concentration. The numerical integrations to evaluate N_A and N_B [24] were performed with Simpson's Rule [41]. The primary components varied were C_A and C_B which are the major determinants of the relative amounts of smaller particles and larger particles in the PSD. The radius which approximately determines which components are dominant, in which size range, is the radius of about 1 μm (2 μm diameter). The smaller A component tends to dominate below this limit and the larger B component

Table 1. Coastal Two-Component Mineral Model Parameters

PSD Model	C_A	C_B	b_A	b_B	μ_A	μ_B	γ_A	γ_B
Prim. Particle Dominant	6.000×10^{23}	1.550×10^{12}	45.0	19.0	3.2	5.0	0.120	0.235
Intermediate Dominance	6.000×10^{22}	1.750×10^{12}	45.0	19.0	3.2	5.0	0.150	0.235
Aggregate Dominant	6.000×10^{23}	1.750×10^{13}	45.0	19.0	3.2	5.0	0.120	0.235

tends to dominate above this limit. The parameters utilized in this study are in Table 1. The changes in the C_A and C_B parameters, generating differing amounts of the relatively small and large particles, were investigated for their effects on the mass-specific scattering cross section, $\sigma_{[PIM]}(\lambda)$.

I assumed that the approximately submicron range, colloidal, mineral particulates represent the A component in the Risović concept of a two component model of the PSD. It is well known that very small colloidal particles aggregate readily and relatively quickly to form particles in the range of about 0.1-1 μm diameter [42–44]. These particles are relatively stable and are distributed in a skewed manner to the larger particle sizes after the smaller particles have been aggregated to form the distribution around a modal diameter of about 1 μm. Such a distribution is a gamma-type or a lognormal-type. Then, various processes, fluid shear, sedimentation, turbulence, etc. combine to slowly form larger, amorphous aggregates from the primary particles generated by aggregation and packing of colloidal particles [33,36,45,46]. Furthermore, Risović and Martinis [22] have related the gamma coefficients (shape parameters) of two-component-type models to the major mechanisms of coagulation and

#155094 - $15.00 USD Received 20 Sep 2011; revised 18 Nov 2011; accepted 1 Dec 2011; published 20 Dec 2011

aggregation. Thus, the B component of a Risović-type two-component model then represents here the relatively amorphous mineral aggregates of greater than 1 μm radius (2 μm diameter). I am calling this the two-component mineral model. About the only data available from the marine environment to compare with these assumptions about the A and B components of a two-component-type model of suspended minerals are those of Green et al. [10], collected from the New England shelf waters. Two distinct mineral particle groupings, particles <3.5 μm and particles >3.5 μm diameter, are evident in their data.

I modeled mineral aggregates of both montmorillonite and illite primary particles. The mineral aggregates were modeled from the fractal-based model of Khelifa and Hill [32]. The refractive indices of Montmorillonite and Illite were used to model the refractive index of the suspended mineral particles. Their refractive indices represent approximate limiting values of the optical properties of the typical clay minerals commonly found in the coastal ocean, with Montmorillonite often the dominant component [47–50]. And, other suspended mineral components have refractive indices close to that of clay minerals [48]. Thus, I assumed that the optical properties of clay minerals would serve as a model of the optical properties of suspended minerals in general. The Khelifa–Hill model was then utilized to determine the relevant physical characteristics of the aggregate particles. Kehlifa-Hill predicts the porosity and density of clay mineral aggregates up to 2000 μm diameter, the aggregates composed of primary particles, 1 μm diameter. It describes an amorphous mineral aggregate with fractal geometry. The fundamental concept of fractal geometry is the fractal dimension that, in this case, summarizes the shape and relative porosity of a mineral aggregate. The fractal dimension is analogous to the dimensions of real objects [46]. The fractal dimension of 3 indicates a 3-dimensional spherical object, tightly packed primary particles perhaps. The Fractal dimension of 2 indicates a 2-dimensional object, which could be considered a "sheet" composed of randomly branching primary particles. The fractal dimension of 1 indicates an object composed of randomly collected particles in a predominantly linear structure. Fractal dimensions in between these limits would then have intermediate structural properties. The fractal dimension F for the clay mineral flocs was determined with the equation

$$F = \alpha \left(\frac{D_f}{d} \right)^{\beta}, \tag{6}$$

where $\alpha = 3.0$, D_f is the equivalent spherical diameter of the floc in μm, D_{fc} is the equivalent spherical diameter of a maximal characteristic floc size, here 2000 μm, F_c is the fractal dimension of the maximal characteristic floc size, d (primary particle diameter) = 1.0 μm, $\beta = \log(F_c/3)/\log(D_{fc}/d)$. The Khelifa-Hill model [32] is expressed as a "median" value and an upper and lower model limit that account for the majority of the experimental and observational values of the clay mineral aggregation studies in their database. These three versions of the model illustrated in Khelifa and Hill [32] were utilized in this study. The model is based on a maximal size for a clay mineral aggregate, an assumed 2000 μm diameter, and a fractal dimension F_c of this maximal aggregate. The fractal dimension for a clay mineral aggregate decreases monotonically from 3.0 for an "aggregate" that is the diameter of the primary particle to the value of F_c for the maximal aggregate diameter. The three model versions are controlled by the value of F_c: 2.4, 2.0, and 1.6, for the maximal aggregate diameter. In turn, these values determine the value of β: – 0.02936,.– 0.0533, and – 0.08270 respectively. The clay mineral aggregate models were referred to as the Low, Standard, and High Khelifa-Hill models. We can see that the dimension of the low fractal limit model predicts an aggregate that is relatively loosely and randomly organized. The high dimension model predicts a more tightly packed clay mineral aggregate. The Khelifa-Hill model then predicts the density of an aggregate or floc based on the fractal modeling of the aggregate. As a floc gets bigger its density becomes lower, i.e. the fractal dimension decreases, and this is important for predicting the settling velocity of the floc and for

#155094 - $15.00 USD Received 20 Sep 2011; revised 18 Nov 2011; accepted 1 Dec 2011; published 20 Dec 2011

estimating the optical properties of the floc [12]. The effective density of the floc is termed the excess density and it was determined from

$$\rho_r - \rho_w = \left(\rho_s - \rho_w\right)\left(\frac{D_f}{d}\right)^{F-3}, \tag{7}$$

where ρ_s = density of the primary particle (montmorillonite or illite), ρ_w = the density of water, ρ_r = the density of the floc (montmorillonite or illite + water). These 3 densities made it possible to construct an optical model of the aggregate proposed by Latimer [31], a coated sphere, of the various sized montmorillonite or illite flocs. Latimer's [31] model consists of the mass of the mineral portion of the floc condensed into a shell of montmorillonite or illite surrounding a core of water. The index of refraction used was that for either montmorillonite or illite and the imaginary components of the refractive indices were determined for the wavelengths utilized, Table 2 [48]. As per Latimer's specifications, coated sphere Mie calculations were performed to determine the scattering efficiency and particle scattering

Table 2. Relative Refractive Indices of Clay Minerals. Real Component n and Imaginary Component n'

Clay Mineral	n	n'								
		412	**440**	**488**	**510**	**532**	**550**	**650**	**676**	**715**
Montmorillonite	**1.17**	1.272 x 10^{-4}	0.900 x 10^{-4}	0.571 x 10^{-4}	0.368 x 10^{-4}	0.323 x 10^{-4}	0.286 x 10^{-4}	0.521 x 10^{-4}	0.677 x 10^{-4}	0.756 x 10^{-4}
Illite	**1.18**	8.433 x 10^{-4}	7.957 x 10^{-4}	7.742 x 10^{-4}	7.190 x 10^{-4}	6.201 x 10^{-4}	5.728 x 10^{-4}	6.928 x 10^{-4}	8.703 x 10^{-4}	9.016 x 10^{-4}

cross section of a floc (B component) of a particular diameter. Fortran code for the Mie calculation of both a solid and a coated sphere came from Bohren and Huffman [51]. The particles of Montmorillonite and Illite, somewhat larger than 1 μm radius, representing the A component, were assumed to be essentially spheres of tightly packed primary particles. Ordinary Mie calculations of a solid homogeneous sphere were performed on the primary clay mineral particles (A component) to determine their scattering efficiencies and particle scattering cross sections. Risović and Martinis [33] demonstrated that the fractal dimension of A component particles in the coastal ocean varied from about 2.7 – 3.0, essentially tightly packed spherical particles or aggregates. The primary particles that contributed the most to the calculation of the mass-specific scattering cross section varied from 0.5 - 3.0 μm radius (1.0 - 6.0 μm diameter) while the most important equivalent spherical radii of the montmorillonite and illite aggregates varied from 2.0 - 8 μm (4.0 - 16 μm diameter). Any primary particles or aggregates larger than those mentioned above did not contribute significantly to the mass-specific scattering cross section. The wavelengths used in the calculations were: 410 nm, 440 nm, 488 nm, 510 nm, 532 nm, 550 nm, 650 nm, 676 nm, and 715 nm.

With all of the information supplied above, we are now ready to calculate theoretically the average mineral mass-specific scattering cross section [52] of a hydrosol $\sigma_{[PIM]}(\lambda)$ and determine its limits. Stavn and Richter [6] derived the theoretical value of the mineral mass-specific scattering cross section determined in the field

$$\sigma_{[PIM]}\left(\lambda\right) = \sum_i \sum_j \left[\frac{\sigma_m\left(\lambda\right)}{\rho_m v_m}\right]_{ij}, \tag{8}$$

where $\sigma_m(\lambda)$ is the particle (primary or aggregate/floc) scattering cross section, here determined from the Mie calculations, λ denotes light wavelength in a vacuum, ρ_m is the

#155094 - $15.00 USD Received 20 Sep 2011; revised 18 Nov 2011; accepted 1 Dec 2011; published 20 Dec 2011

mineral density, either as primary particle or as a floc, v_m is the volume of either a primary mineral particle or of a mineral aggregate, i subscript indicates summation over particle species, j subscript indicates summation over the weighted size classes of a particular mineral species. I utilized mineral mass-specific scattering cross sections from Mobile Bay, Alabama, USA, Southwest Pass, mouth of the Mississippi, USA [6], and the Irish Sea, UK [37,38] to compare with the theory.

3. Results

The two-component mineral model particle size distribution dominated by primary particles is

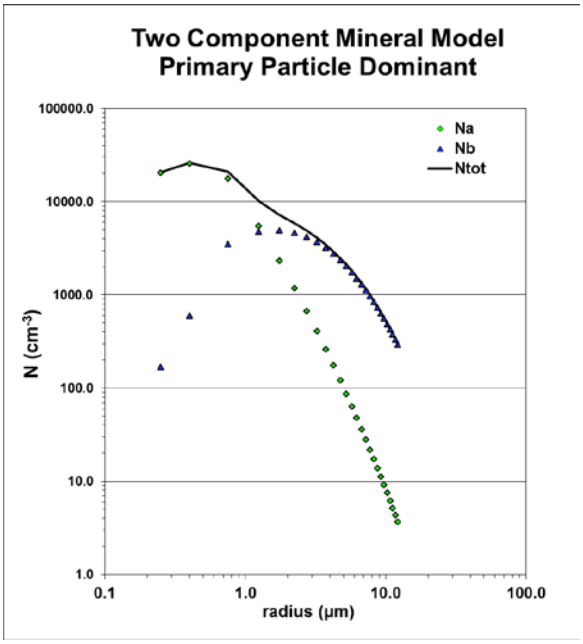

Fig. 1. Particle size distribution for primary mineral particle dominated PSD. The ratio of small particles to large in this model is $N_A/N_B = 1.55$. The parameters of the Two-component Mineral Model applied here are: $C_A = 6.0 \times 10^{23}$, $C_B = 1.55 \times 10^{12}$, $\mu_A = 3.2$, $\mu_B = 5.0$, $\gamma_A = 0.12$, $\gamma_B = 2.35$

plotted in Fig. 1. The dominance by primary particles is indicated by the ratio $N_A/N_B = 1.55$. The distribution of the mineral aggregates of component B occurs at least one order of magnitude lower than the peaked portion of the distribution of primary particles, component A. The particle size distribution in which the primary particles and the aggregate particles are of about the same order of magnitude concentration is plotted in Fig. 2. The near equivalence

#155094 - $15.00 USD Received 20 Sep 2011; revised 18 Nov 2011; accepted 1 Dec 2011; published 20 Dec 2011

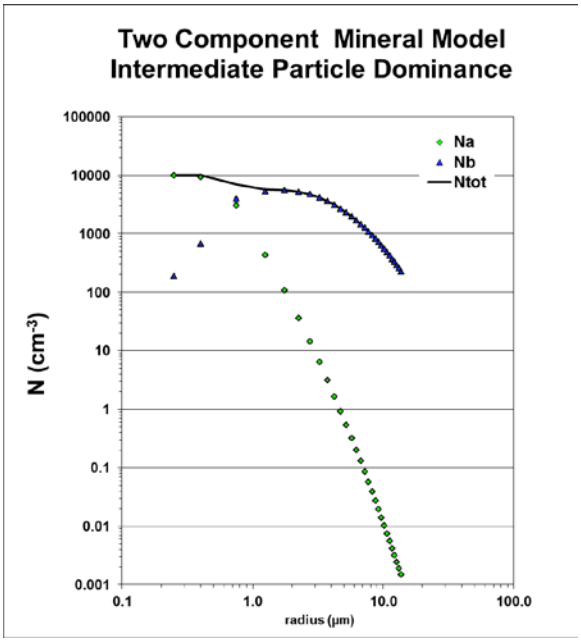

Fig. 2. Particle size distribution for equivalent primary and aggregated mineral PSD. The ratio of small particles to large in this model is $N_A/N_B = 0.42$. The parameters of the Two-component Model applied here are: $C_A = 6.0 \times 10^{22}$, $C_B = 1.75 \times 10^{12}$, $\mu_A = 3.2$, $\mu_B = 5.0$, $\gamma_A = 0.15$, $\gamma_B = 2.35$

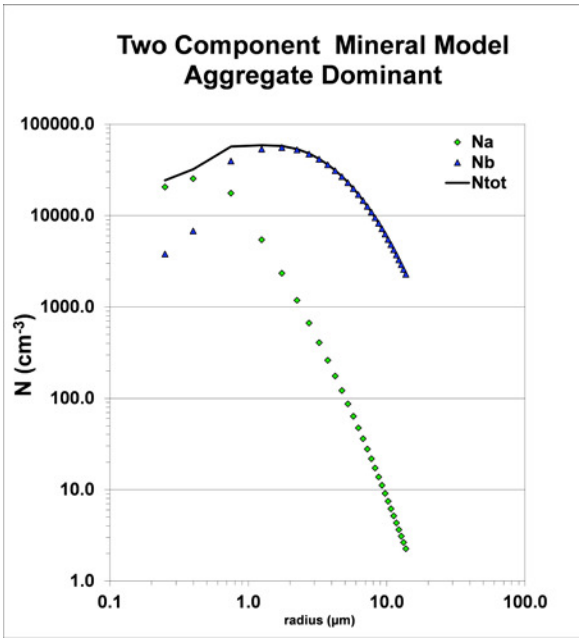

Fig. 3. Particle size distribution for mineral aggregate dominated PSD. The ratio of small particles to large in this model is $N_A/N_B = 0.135$. The parameters of the distribution applied here are: $C_A = 6.0 \times 10^{23}$, $C_B = 1.75 \times 10^{13}$, $\mu_A = 3.2$, $\mu_B = 5.0$, $\gamma_A = 0.12$, $\gamma_B = 2.35$

of primary particles and aggregated particles is indicated by the ratio $N_A/N_B = 0.42$. The particle size distribution that is dominated by mineral aggregates is plotted in Fig. 3. The

#155094 - $15.00 USD Received 20 Sep 2011; revised 18 Nov 2011; accepted 1 Dec 2011; published 20 Dec 2011

mineral aggregates occur at significantly greater concentration than the primary mineral particles, indicated by the ratio N_A/N_B = 0.135, nearly an order of magnitude higher. The essential difference between these distributions is the C_A/C_B ratio (Table 2) which serves to simply move the distribution of the mineral aggregates, component B, up or down relative to the distribution of primary particles, component A, and redistribute the particle concentrations. It is possible to see that the log plot of total particles with radius, in some cases, could be interpreted as a constant slope in some sections of the distribution, especially the larger radii (Figs. 1-3).

Mineral mass-specific scattering cross sections $\sigma_{[PIM]}(\lambda)$ calculated from the aggregate models utilized here (PSD's delineated in Figs. 1-3) and field data [6] with new correction factors are plotted in Figs. 4 and 5 and the comparisons with Irish Sea data [37,38] are in Fig. 6. In Fig. 4 we compare the calculated plots of $\sigma_{[PIM]}(\lambda)$ for the primary particle dominated PSD with the $\sigma_{[PIM]}(\lambda)$ plot for Mobile Bay, Alabama, USA. The values of $\sigma_{[PIM]}(\lambda)$ in Mobile Bay varied from 0.84 – 0.64 m^2 g^{-1}, from the blue to the red end of the spectrum, and

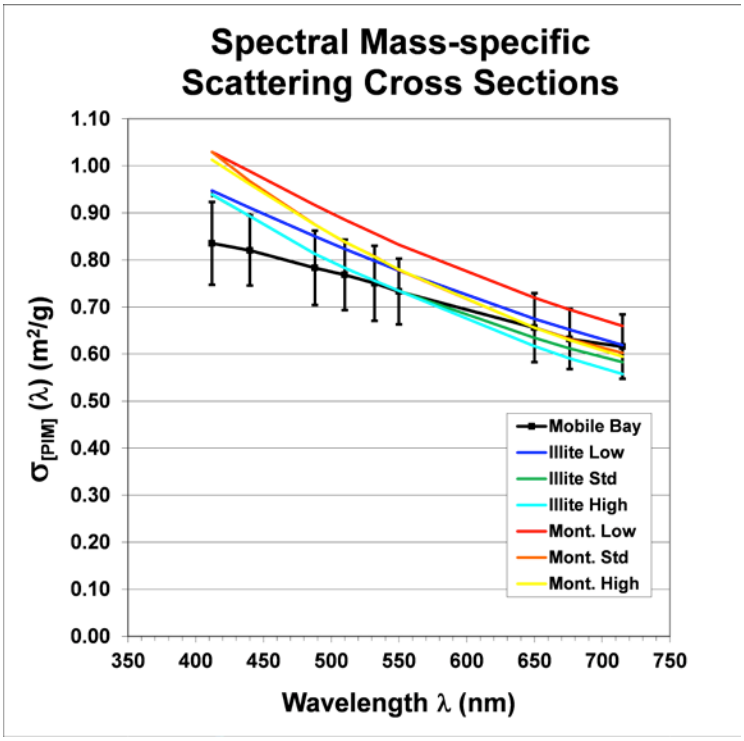

Fig. 4. Mass-specific scattering cross sections for primary particle dominated PSD compared to Mobile Bay, Alabama, USA results (Stavn and Richter, 2008). Results from Montmorillonite and Illite aggregate models determined at low, median, and high fractal dimensions.

these values were the highest of any field data recorded. The plots from all the models demonstrate values of $\sigma_{[PIM]}(\lambda)$ of 1.03–0.59 m^2 g^{-1} from the blue to the red end of the spectrum. Most of the model values tend to fall above the values of the field data. All the model plots fall within the standard errors for the field data at the wavelengths 650 nm – 715 nm. The Montmorillonite Low Model falls above the standard error of the field data at all shorter wavelengths. All models fall above the standard error of the field value at 412 nm. All models except the Montmorilllonite Low Model just equal or fall inside the upper standard error value at the wavelengths of 488 nm – 550 nm. The spectral slopes for models and field data appear to be comparable, are negative from the blue to the red end of the spectrum, and

#155094 - $15.00 USD Received 20 Sep 2011; revised 18 Nov 2011; accepted 1 Dec 2011; published 20 Dec 2011

appear to be the largest slopes recorded from the field. The extreme model values are represented by the Montmorillonite Low Model and the Illite High Model. The closest fits appear to be Illite in either the Standard or High Models.

In Fig. 5, we compare the plots of $\sigma_{[PIM]}(\lambda)$ from the intermediate particle PSD to the plot from Southwest Pass, Mississippi River, USA. The values of $\sigma_{[PIM]}(\lambda)$ at the Southwest Pass varied from 0.63 – 0.51 $m^2\ g^{-1}$, from the blue to the red end of the spectrum, and these values

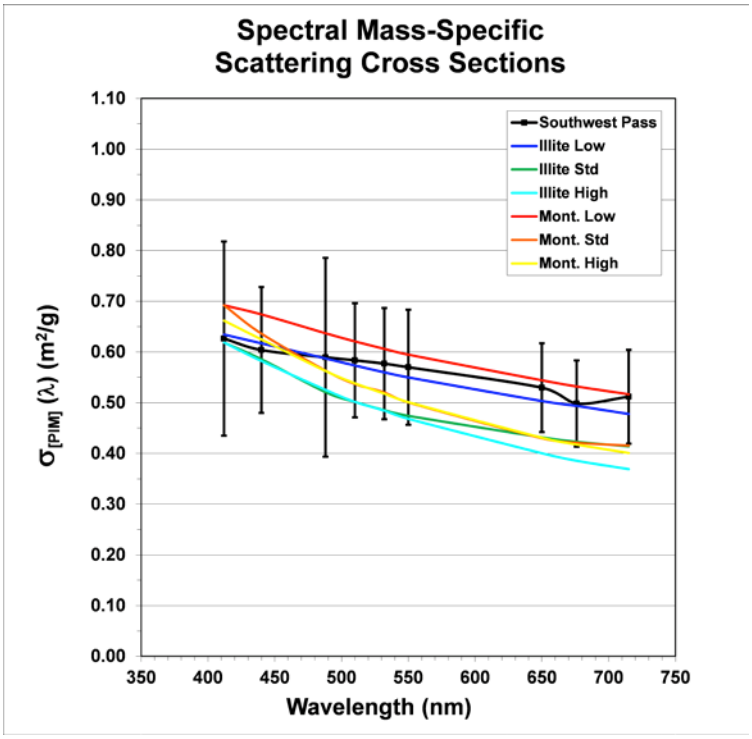

Fig. 5. Mass-specific scattering cross sections for primary and aggregate co-dominant PSD and compared to Southwest Pass, mouth of the Mississippi, USA data (Stavn and Richter, 2008). Results from Montmorillonite and Illite aggregate models determined at low, median, and high fractal dimensions.

were in the mid-range of any recorded from the field. The plots from all the models demonstrate values of $\sigma_{[PIM]}(\lambda)$ of 0.69 – 0.37 $m^2\ g^{-1}$ from the blue to the red end of the spectrum. All of the model plots fall within the standard errors determined for the field data with the exception of the Illite High and Montmorillonite High Models at 676 nm and 715 nm. Most of the model values tend to fall below the values of the field data. The spectral slopes for models and the field data appear to be comparable with the Illite Low Model and the Montmorillonite Low Model having slopes closest to the field data. The spectral slopes are negative from the blue to the red end of the spectrum and they appear to be less than the spectral slopes for the primary particle dominant PSD in Fig. 4. The extreme model values are represented by the Montmorillonite Low model and the Illite High model. The closest fit appears to be the Illite Low model.

In Fig. 6, we compare the plots of calculated $\sigma_{[PIM]}(\lambda)$ values from the aggregate dominated PSD models with two plots of field data from the Irish Sea, UK [37,38]. The values of $\sigma_{[PIM]}(\lambda)$ from the Irish Sea vary from approximately 0.23 to 0.34 $m^2\ g^{-1}$ at the blue

#155094 - $15.00 USD Received 20 Sep 2011; revised 18 Nov 2011; accepted 1 Dec 2011; published 20 Dec 2011

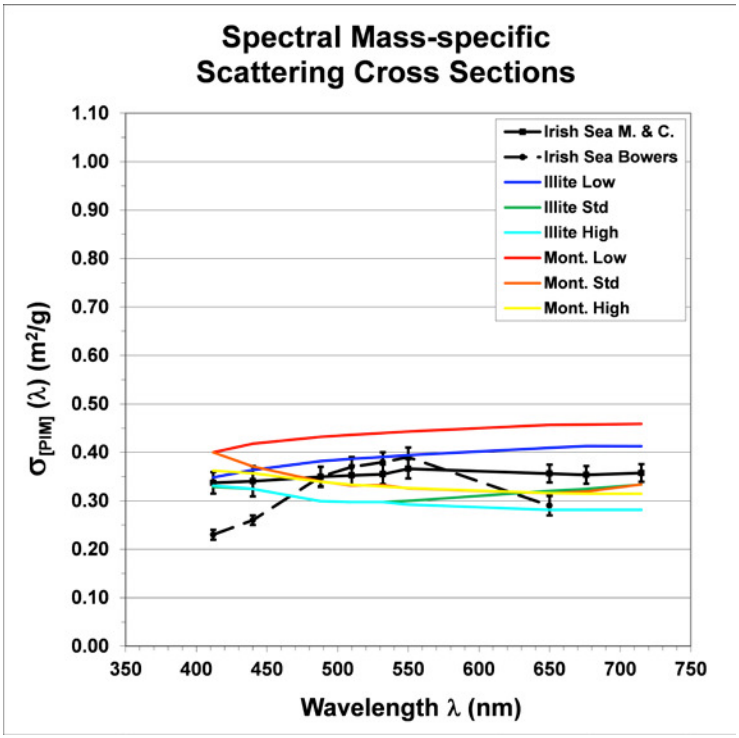

Fig. 6. Mass-specific scattering cross sections for aggregate dominated PSD compared with results from the Irish Sea (Bowers and Binding, 2006, McKee and Cunningham, 2006). Results from Montmorillonite and Illite aggregate models determined at low, median, and high fractal dimensions.

end of the spectrum to 0.29 to 0.36 m^2 g^{-1} at the yellow/red end of the spectrum and these are the lowest recorded field values. The values from aggregate dominated PSD models for $\sigma_{[PIM]}(\lambda)$ cluster reasonably closely around the Irish Sea data but no model settles completely within the standard deviation limits of the field data. The field data indicate either no significant spectral slope to the Irish Sea data or perhaps a positive spectral slope from the blue to the red end of the spectrum. In addition, there is a possible spectral peak in the region around 550 nm in the field data. The model calculations tend to fall equally above and below the field data. The extreme values from the model calculations occur with the Montmorillonite Low Model to the Illite High Model. The Illite Low Model appears have a spectral slope comparable to the data from Mckee and Cunningham [38] and for the most part hovers just above the standard deviation limits of the data. The Illite Low Model calculations fit within the standard deviation limits of the middle portion of the Bowers and Binding [37] data. The calculations from the Montmorillonite Low Model demonstrate a comparable spectral slope. There is an interesting “hinge point” with the model calculations in which the spectral slopes are either small to 0 or varying between being negative or positive The field data reported from Bowers and Binding [37] are comparable to much of the data of McKee and Cunningham [38] but diverge somewhat at at the blue and yellow/red ends. There is a positive spectral slope to the Bowers and Binding [37] data if we discount the data point at 650 nm

4. Discussion

We have demonstrated theoretical characteristics of the mass-specific scattering cross section of suspended mineral matter that are verified in part by experimental observations from field

#155094 - $15.00 USD Received 20 Sep 2011; revised 18 Nov 2011; accepted 1 Dec 2011; published 20 Dec 2011

studies and this will have practical applications. I have proposed a two-component mineral PSD model based on Risović's two-component model for the total particle PSD. The smaller (A) component of the two-component mineral model is assumed to be primary mineral particles. The larger (B) component of the PSD model is assumed to be aggregates composed of the primary particles. The results presented here will potentially apply to all studies of suspended mineral matter in the coastal ocean and inland waters.

The rationale of the models is as follows. In an effort toward sensitivity analysis, I have applied the refractive indices of Montrmorillonite and illite, as possible mid values of mineral real refractive indices [11,53]. The imaginary components of their refractive indices [11] may serve as typical limiting values of the mineral refractive index. Thus I have montmorillonite and illite models which serve as models for the refractive index of suspended mineral matter. The aggregation of primary clay mineral particles to secondary mineral aggregates is modeled from the Khelifa-Hill [32] clay mineral fractal aggregation model. The Khelifa-Hill model for clay mineral aggregations was expressed in three forms, based primarily on variations in the fractal dimension of the largest aggregate particle in the model, assumed to be 2000 μm in this study. The fractal dimensions for the maximum diameter clay mineral aggregate in their model were 2.4, 2.0, 1.6. I proposed three models based on the three fractal dimensions of Khelifa and Hill [32]. The High Model (maximum fractal dimension 2.4) aggregates are a series that tends to be relatively more tightly packed with primary clay mineral particles. The Standard Model (maximal fractal dimension 2.0) aggregates are a series that is more diffuse and open. Finally, the Low Model (maximal fractal dimension 1.6) aggregates are a series with the most open and loosely packed aggregate structures. Latimer [31] provides accurate estimates of the physical and optical properties of the clay mineral aggregates (B component) based on the variations in the models delineated above and the optical coated sphere model. Changes applied to the parameters of the two-component mineral model were, in part, designed to mimic the changes occurring in suspended mineral particles associated with the process of mineral particle aggregation. The extended gamma distribution provided the basis for the distribution of component A, the primary clay mineral particles. Another extended gamma distribution provided the basis for component B, the model for the distribution of aggregated primary clay mineral particles. The gamma distribution parameters reported by Risović [24] were used as a starting point. The C_A and C_B coefficients are directly related to the concentrations of primary and secondary (aggregated) particles, Eqs. (3) and (4). In addition to the magnitudes of C_A and C_B, Eqs. (3) and (4) demonstrate that the relative concentrations of the A and B components are also a function of their respective gamma or distribution shape coefficients. The C_A coefficient and the C_B coefficient were varied to simulate the process of aggregation of primary particles into secondary particles or aggregates by decreasing the A component and increasing the B component. The particle distributions varied from one with primary particles dominant, relatively smaller C_B coefficient, to one of aggregated particles being dominant, with a relatively large C_B coefficient (Table 1). The shapes of the two components were nearly constant and only their positions in the total distribution relative to each other varied. Thus the number of aggregated primary particles increased in the three PSD's utilized (Figs. 1-3). The change in absolute number concentrations of the A and B components without change in shape of the component distributions would mimic one process or series of constant processes creating aggregates from primary particles (concentration decreasing) and the size classes of the B component increasing proportionately. This change in the relative concentrations of A and B components creates an increase in the size of the modal class of the total particle distribution (Figs. 1-3). The two-component extended gamma distribution of suspended mineral components, emulating the Risović two-component total particle distribution, proved capable of reproducing the values of $\sigma_{[PIM]}(\lambda)$ recorded in the field.

The mass-specific scattering cross sections of Mobile Bay, Alabama, USA, were the highest values reported in this study (Fig. 4). Intercomparisons of scattering data are often

#155094 - $15.00 USD Received 20 Sep 2011; revised 18 Nov 2011; accepted 1 Dec 2011; published 20 Dec 2011

formulated in the region of 550 nm, roughly the middle of the visible spectrum, and this works well for mineral scattering as there aren't usually multimodal peaks in the spectral slope for mineral scattering. For Mobile Bay, the value of $\sigma_{[PIM]}(550)$ is about 0.74 m^2 g^{-1}. The $\sigma_{[PIM]}(550)$ model values ranged from about 0.83-0.74 m^2 g^{-1}, tending to be higher than the field values. Only the highest model value fell outside the standard error limits of the field value. The association of high values of $\sigma_{[PIM]}(\lambda)$ with a fairly steep spectral slope comes from a suspended mineral particle distribution dominated by the small primary particles of Component A (Figs. 1, 4). In Fig. 1 the modal class for suspended mineral particles appears to be about 0.5 μm radius (1.0 μm diameter). Thus we can infer that the suspended minerals of Mobile Bay are not significantly aggregated and exist for the most part as primary clay mineral particles. It is possible that a mineral model with greater width of the component distributions would have a smaller and/or flatter spectral slope, like the field data, a subject for future theoretical and experimental investigations. At Southwest Pass, mouth of the Mississippi, USA, the mass-specific scattering cross section was lower in value and the spectral slope was a little flatter than that at Mobile Bay (Fig. 5). The value of $\sigma_{[PIM]}(550)$ is about 0.58 m^2 g^{-1}. The $\sigma_{[PIM]}(550)$ model values range from about 0.59 m^2 g^{-1} to 0.47 m^2 g^{-1}, tending to be lower than the field values. All model values fell within the standard error limits. The lower value of $\sigma_{[PIM]}(\lambda)$ and the flatter spectral slope are associated with a suspended mineral particle distribution in which smaller primary clay mineral particles (Component A) are approximately co-dominant with aggregated clay mineral particles (Component B), Fig. 2. The approximate modal size class of the total PSD appears to cover a plateau from about 0.8 μm to about 1.0 μm radius (1.6 μm to about 2.0 μm diameter), Fig. 2. Overall, considering the pattern of the results, the models for primary particle dominant systems may have had a modal particle class somewhat smaller than those of Mobile Bay. The model for a co-dominant system may have had a larger modal particle class than was the case for Southwest Pass. Illite in a fairly well-packed aggregate appears to mimic well the data for Mobile Bay. Both Illite and Montmorillonite in a loosely packed aggregate appear to mimic well the Southwest Pass field data.

The final sets of field data presented here come from the Irish Sea, UK, as reported by Bowers and Binding [37] and McKee and Cunningham [38], Fig. 6. These were the lowest recorded field values of the mass-specific scattering cross section. The value of $\sigma_{[PIM]}(550)$ is about 0.38 m^2 g^{-1}.to 0.39 m^2 g^{-1}, both values easily falling within the standard deviation of the other (Fig. 6). Furthermore, the field data demonstrate the possibility of a "bulge" at 550 nm in the green spectral region. The $\sigma_{[PIM]}(550)$ model values vary from about 0.44 m^2 g^{-1} to 0.29 m^2 g^{-1}, about equally above and below the field values. The lowest values for $\sigma_{[PIM]}(\lambda)$ and the spectral slope varying from zero to positive are associated with a suspended mineral particle distribution in which the aggregated clay mineral particles (Component B) are dominant (Fig. 3). The approximate modal size class of the total PSD appears to be at the radius of 2.0 μm (4.0 μm diameter), Fig. 3. At this stage we have qualitative and partial quantitative agreement of the field studies and the theoretical results reported here when we consider the magnitude of $\sigma_{[PIM]}(\lambda)$. In the theoretical studies, however, the spectral slope of the mass-specific scattering coefficient is changing depending on the fractal dimension of the models generated. The montmorillonite and illite models with the lowest fractal dimension, and therefore the loosest, most open, aggregates, demonstrate a positive spectral slope. The comparable clay mineral models with a more tightly packed clay mineral aggregate (higher fractal dimension) exhibit a negative spectral slope. The Irish Sea is a relatively shallow shelf sea experiencing significant tidal and turbulent resuspension of bottom sediments [37,54]. Thus we see a coastal system exhibiting relatively large amounts of aggregated clay minerals that depress the value of $\sigma_{[PIM]}(\lambda)$ and tend to form a broad "green peak" or simply a generally positive spectral slope. There are many possible factors to explain the phenomenon of increased scattering in the middle of the visible spectrum by clay minerals and one is the absorptive component of the clay mineral refractive index. Table 2 demonstrates that the imaginary

#155094 - $15.00 USD Received 20 Sep 2011; revised 18 Nov 2011; accepted 1 Dec 2011; published 20 Dec 2011

component of the clay mineral refractive index is lower in the green portion of the spectrum than in either the red or blue ends. Overall, relatively greater amounts of larger secondary clay mineral aggregates will decrease the value of $\sigma_{[PIM]}(\lambda)$ and tend to either flatten the spectral slope or yield a positive spectral slope from the shorter to the longer wavelengths. An illite model that is relatively loosely packed tends to mimic the positive spectral slope of $\sigma_{[PIM]}(\lambda)$ reported by McKee and Cunningham [38] (Fig. 6) while more tightly packed montmorillonite exhibits more values within the standard deviation of the McKee and Cunningham [38] data and exhibiting a flatter slope.

There is a series of experimental studies that have a bearing on what we have reported here [19–21]. These studies report primarily on the mass-specific scattering coefficient, an empirical ratio of the total particle scattering coefficient and the total concentration of suspended matter, both mineral and organic. Thus the empirical ratio is not exactly defined optically, as is done in Eq. (8) and Stavn and Richter [6], but this empirical ratio can approach the exactly defined values of Eq. (8). Stramski et al. [21] performed experiments on clay minerals suspended in sea water and these values are a close approximation to an exactly defined and investigated mass-specific scattering cross section. These suspensions were not corrected for the presence of organic matter in suspension with the clay minerals. The majority of the experiments are performed on air dust samples that have not been analyzed as to the type of minerals in the dust and the amount of organic materials in the dust such as black carbon. Another factor that renders the experimental ratios less than comparable with what is reported here is that suspended minerals, being dense, are notoriously difficult to work with and maintain in a stable, repeatable state in suspension [44]. Therefore, many of the reported experimental results may simply be a function of how a particular suspension of minerals or dust was prepared and handled. The particle size distributions for the suspensions were determined with a Coulter counter which has unknown effects on the aggregation state of suspended particles, a major topic of investigation here.

Mass-specific scattering coefficients were reported in Stramski et al. [21] for montmorillonite, illite, and calcite that closely approached $\sigma_{[PIM]}(\lambda)$ values as reported in this study, defined in Eq. (8). The values approximating $\sigma_{[PIM]}(\lambda)$ for calcite in the range 400 nm to 700 nm were 1.6 – 1.2 $m^2\ g^{-1}$ for a small particle dominated PSD and 1.18 – 0.92 $m^2\ g^{-1}$ for a large particle dominated PSD, both of which had a negative spectral slope. These values tend to bracket the $\sigma_{[PIM]}(\lambda)$ for calcite liths of approximately 1.0 μm equivalent spherical diameter reported in Stavn and Richter [6]. A negative spectral slope was recorded for both montmorillonite and illite suspensions [21] with a mass-specific scattering coefficient of 0.84 – 0.63 $m^2\ g^{-1}$ for 412 nm – 715 nm which accords well with the $\sigma_{[PIM]}(\lambda)$ values reported for Mobile Bay [6] and the theoretical calculations in Fig. 4. These results of Stramski et al. [21] were recorded for a large particle PSD. There were no flat spectral slopes for the mass-specific scattering coefficients of mineral suspensions but there were flat spectral slopes reported for the mass-specific scattering coefficients of air dust suspensions. The approximate value for Sahara Dust across the visible spectrum was 0.75 $m^2\ g^{-1}$ which is higher than the nearly flat spectral values for $\sigma_{[PIM]}(\lambda)$ reported from the Irish Sea and our theoretical calculations in Fig. 6. From the results of this report it appears that a large value of a flat spectrum could be attributed to very loosely packed aggregate particles of the air dust. Stramski et al. [21] also state the possibility that scattering by relatively small mineral particles might have been coupled with strong absorption in the blue region of the spectrum by organic matter to yield a relatively flat spectrum for the mass-specific scattering coefficient. Also, lower values of the mass-specific scattering coefficient that accord with the results of Fig. 6 were reported by Stramska et al. [19] for air dust samples that were not allowed to settle as had been the case for the earlier reports [20,21]. This sample treatment retained larger particles but the difficulties of maintaining stable mineral suspensions were indicated in the erratic, highly variable values of the optical coefficients for these suspensions. Reversal of the spectral slope of the mass-specific scattering coefficients to a positive spectral

#155094 - $15.00 USD Received 20 Sep 2011; revised 18 Nov 2011; accepted 1 Dec 2011; published 20 Dec 2011

slope was not reported. However, the spectral slope of the mass-specific scattering coefficient for Oahu Air Dust reported in Stramski et al. [21] indicates a possible positive spectral slope from 400 nm – 650 nm with a tendency to flatten at longer wavelengths. In this study we have reported a reversal of spectral slope in the field data of the Irish Sea and in our theoretical calculations of $\sigma_{[PIM]}(\lambda)$.

The results of this study may have a bearing on a discussion in the literature concerning the spectral slope of the marine hydrosol scattering coefficient, which is primarily affected by the suspended particulates of the hydrosol. Gould et al. [39] report that the hydrosol scattering coefficient of the coastal ocean has a negative spectral slope, from the blue to the red end of the spectrum. This spectral slope decreases as one goes from the coastal ocean to the clear water of the open ocean. Others have reported difficulty in reproducing this result [55] even though Gould et al. [39] quote similar studies from sediment-laden river mouths, etc. The results of Gould et al. [39] were from readings taken in the upper 1.5 meters while others, Barnard et al. [55], took optical readings from the surface to the bottom. It is entirely possible, in the case of the coastal ocean, that near surface samples such as from Gould et al. [39] would be dominated by smaller primary mineral particles that would sink slowly compared to larger aggregates. We have demonstrated that in a mineral dominated system of mostly smaller primary mineral particles (Fig. 4) one would expect a negative spectral slope for the scattering coefficient. Furthermore, sinking aggregates can grow in size in the process of aggregation by differential sedimentation which would increase the relative contribution of the B component (larger particles) of the PSD.to the scattering coefficient [22]. These mineral aggregates, if dominant, would generate a smaller spectral slope to none to possibly a positive spectral slope (Figs. 5,6). This might explain the discrepancies reported in the above studies.

5. Conclusions

The mineral spectral mass-specific scattering cross section, $\sigma_{[PIM]}(\lambda)$, has been shown to be remarkably sensitive to particle size. The presence of small mineral particles in the range of 0.5 μm - 3.0 μm radius (1 μm - 6.0 μm diameter) is most strongly indicated in the numerical values of $\sigma_{[PIM]}(\lambda)$. Stavn and Richter [6] using Eq. (8) for lith plates from Coccoliths (0.5 μm equivalent spherical radius) and the data of Gordon and Du [56] determined that a monodispersion of lith plates would have a $\sigma_{[PIM]}(550)$ value of 0.98 m^2 g^{-1}. As the relative number of small particles decreases the value of $\sigma_{[PIM]}(\lambda)$ decreases as shown in the values for $\sigma_{[PIM]}(550)$ quoted in the discussion, 0.74, 0.58, 0.38 m^2 g^{-1} for the field data reported. Comparable values were demonstrated in the theoretical calculations of $\sigma_{[PIM]}(\lambda)$ for PSD's with increasing size of modal particle class (Figs. 4-6). This is true because as particles get larger, their equivalent spherical cross sections increase approximately as the square of an equivalent spherical radius but their masses increase as the cube of their equivalent spherical radiuses. The particle mass is, of course, in the denominator of the expression for $\sigma_{[PIM]}(\lambda)$ in Eq. (8). However, a mineral aggregate actually contributes more to $\sigma_{[PIM]}(\lambda)$ than a solid equivalently spherical particle of the same radius because the aggregate, composed of a certain percentage of primary particles in an open structure that includes water, is less dense than the equivalent solid particle. Along with the decrease in magnitude of $\sigma_{[PIM]}(\lambda)$, its spectral slope also decreases (Figs. 4-6). The field evidence indicates that the spectral slope of $\sigma_{[PIM]}(\lambda)$ for suspended mineral particulates becomes zero or positive (Fig. 6) as the value of $\sigma_{[PIM]}(\lambda)$ decreases. The theoretical calculations involving clay mineral aggregates (Fig. 6) indicate a reversal of spectral slope as the clay mineral aggregate becomes less tightly packed by primary particles (the fractal dimension decreases). The spectral slope for the relatively tightly packed aggregate models remained negative or approached zero (Fig. 6). The best fitting models for the field data were relatively tightly packed when the particles were dominated by the primary (A) component. As the aggregates increased in importance, the best fitting models were the loosely aggregated ones. Thus $\sigma_{[PIM]}(\lambda)$ is also sensitive not only to the increase in size of mineral aggregates but also to their fractal dimension or degree of packing.

#155094 - $15.00 USD Received 20 Sep 2011; revised 18 Nov 2011; accepted 1 Dec 2011; published 20 Dec 2011

The presence of significant mineral aggregates will slowly lower the value of $\sigma_{[PIM]}(\lambda)$, flatten or reverse the sign of the spectral slope, and may create a peak value in the green region, about 550 nm, of the spectrum if the slope tends to level off at longer wavelengths as may be indicated by the Irish Sea data (Fig. 6).

Both montmorillonite and illite appear to provide usable models of the refractive index of suspended mineral particles and mineral aggregates. More field data may allow the determination of a reasonable "average" value for the refractive index of suspended mineral matter for the purposes of biogeo-optical modeling of the coastal ocean and providing new, accurate remote sensing algorithms for the coastal ocean. The clay mineral aggregate model of Khelifa and Hill [32] has provided valuable insights into when the degree of "packing" of an aggregate, expressed as the fractal dimension, may have a bearing on the magnitude and the slope of the mass-specific scattering cross section. In addition, the two-component mineral model, inspired by Risović's two-component total particle formulation, utilizing the extended gamma distribution for the PSD of the suspended particles, gives us great flexibility in investigating the dynamics of particle aggregation and their effects on hydrosol optical properties [22].

Acknowledgments

D. Risović provided valuable support and comment for this project. Emmanuel Boss and Rebecca Green provided helpful comments on the topics covered in this report. Emmanuel Boss especially made me aware of the important optical work of Latimer. Further support came from the Naval Research Laboratory, Program Element 61153N for Richard W. Gould, Jr., Code 7331, Bio-optical Physical Processes and Remote Sensing Section. This report is NRL Contribution Number: NRL/JA/7330 – 11-0882

#155094 - $15.00 USD Received 20 Sep 2011; revised 18 Nov 2011; accepted 1 Dec 2011; published 20 Dec 2011